Quadratic Mixed Convection Tangent Hyperbolic Stratified Fluid Flow Past a Vertical Elongated Sheet with Nonlinear Thermal Radiation: Spectral Local Linearization Method

A. J. Adigun[1*], E. O. Fatunmbi[2], C. U. Boneze[3]

1 Department of Mathematical Sciences, University of Delaware, USA.
2 Department of Mathematics and Statistics, Federal Polytechnic, Ilaro, Nigeria.
3 Department of Mathematics, University of Louisiana, USA.
* Corresponding author: aanuadig@udel.edu, ephesus.fatunmbi@federalpolyilaro.edu.ng, chikaboneze1@louisiana.edu

Abstract

In the present study, the flow of tangent hyperbolic fluid over a vertically elongated sheet with double stratification and nonlinear thermal radiation effects is investigated. The model is developed with nonlinear mixed convection of second-order via Boussinesq approximation, a transverse magnetic field of uniform strength, viscous dissipation effects and temperature-dependent thermal conductivity. The model equations are transformed from nonlinear partial differential equations into ordinary differential equations through appropriate similarity transformation quantities while the translated equations are solved with an iterative technique known as the Spectral Local Linearization Method (SLLM). A comparison of the obtained results in the current study with related existing studies in the literature shows perfect agreement under some limiting constraints. The physical parameters' effects on the dimensionless velocity, temperature, skin friction coefficient and Nusselt number are clearly illustrated by various graphs. In the analysis, it is found that an increase in the fluid material parameter decelerates the fluid motion while the velocity appreciates with the mixed convection term. Similarly, the surface heat transfer improves by raising the value of the temperature ratio parameter (nonlinear thermal radiation) whereas there is a reduction in the heat transfer in the presence of the thermal stratification parameter.

1   Introduction

Due to their numerous applications in the fields of science, engineering, and technological progress, non-Newtonian fluids have become indispensable in all spheres of human endeavor. For instance, the

extrusion of polymers, the production of cosmetics, the extraction of crude oil, the production and processing of food, and the production of drugs and pharmaceuticals [1]. Owing to the diversity of fluid characteristics in nature, it is no longer feasible to include all of the properties of non-Newtonian fluids in a single constitutive model; consequently, various models of non-Newtonian fluids exist based on their physical attributes. Existing fluid models for non-Newtonian fluids include the tangent hyperbolic fluid, Casson fluid, micropolar fluid, Jeffrey fluid, Maxwell fluid, Powell-Eyring, Prandtl-Prandtl fluid, viscoelastic fluid, etc. The model for tangent hyperbolic fluid stands out due to its simplicity and applicability, which has piqued the interest of numerous researchers. It is a property of non-Newtonian fluids that viscosity degenerates with increasing shear rate, according to Jabeen et al. [4]. Experiments with fluids such as ketchup, pigments, melts solution, and polymers reveal such characteristics. In biological fluids (such as blood), the shear-thinning property of circulating blood prevents coagulation from obstructing capillaries and arteries. In addition, its constitutive equation was derived from the molecular kinetic theory, as opposed to the empirical relations used in other fluid models. Due to these intriguing rheological properties, quite a few researchers have applied tangent hyperbolic fluid models to various geometries with varying wall conditions and hypotheses. Ullah et al. [5] examined numerically the MHD tangent hyperbolic fluid transport model over a stretching sheet under the influence of suction/injection. The numerical analysis reveals that fluid motion decreases as the power law index and Weissenberg number increase. Mahdy [6] analyzed a continuous flow of hydromagnetic tangent hyperbolic fluid containing minute nanoparticles over an elongated cylinder with variable wall temperature conditions and entropy analysis. Salahuddin et al. (7) modeled the stagnation-point flow of tangent hyperbolic fluid past an extending cylinder with varying thermal conductivity and viscosity. Ibrahim [8] reported numerically on this phenomenon over an extending sheet with zero mass flux, thermal radiation, heat convective boundary condition, and second-order slip.

In high-temperature manufacturing and engineering processes, such as those used in nuclear power plants, hot rolling, heat exchangers, and electrical power generation, it's crucial to have a precise understanding of thermal radiation to develop efficient energy conversion devices. The development of radiative heat flux in the energy equation can be either linear or nonlinear, depending on the temperature intensity in the flow region. Adeniyan and Adigun [9,10] and Alao et al. [11] have shown that the linear radiative heat flux is applicable when the temperature difference within the flow is low, while the nonlinear type is necessary to predict accurately when the temperature difference is large. Kumar et al. [12] have studied the effect of thermal radiative flux on the slip transport of Carreau fluid mixed with nanoparticles, and their numerical investigation has demonstrated that the heat transfer improves as the radiation and temperature ratio term increases. Rana et al. [13] have investigated a similar concept in an unsteady reactive nanofluid flow past a linearly stretching material towards a stagnation point. To numerically analyze the nonlinear thermal radiative effects and entropy analysis over a stretchable sheet being influenced by variable properties of a micropolar fluid, Fatunmbi and Adeniyan [14] have conducted a study. Gbadeyan et al. [15] have evaluated the combined effects of nonlinear thermal radiation, variable thermal conductivity, and viscosity on the movement of boundary layer Casson fluid past a convectively heated vertical porous plate, while Yusuf et al. [16] have studied this phenomenon on a hybrid nanofluid. Most recently, Fatunmbi et al. [17] have assessed the impact of viscous dissipation and nonlinear thermal radiation on the flow and heat transfer of Eyring-Powell nanoliquid over a magnetized Riga plate with varying heat conductivity.

The combined natural and forced convection is often referred to as mixed convection. There are applications of such a phenomenon which include; drying processes, lubrication grooves, ocean and reservoirs, cooling of fans and electronic appliances, solar power collectors, etc. Various authors in the past have proposed linearity assumption for the density variation with temperature in the buoyancy force term of the momentum equation. Meanwhile, the existence of a large temperature difference between the surface and the ambient necessitates a nonlinear density variation with temperature and concentration. Based on this, Fatunmbi et al. [18] examined such a concept in a reactive tangent hyperbolic nanoliquid in the neighbourhood of a stagnation point over a nonlinear stretching surface using the shooting technique. The motion of nonlinear mixed convection

nanoliquid past an accelerated vertical cylinder is presented by Patil et al. [19] in the presence of viscous dissipation. Alsaedi et al. [20] analytically evaluated hydromagnetic Eyring-Powell nonlinear mixed convection flow with the impact of Joule heating and viscous dissipation. It was reported that the growth in the mixed convective variable enhanced the velocity due to the dominance of the buoyancy force over the viscous force. None of these studies however has been conducted to examine the impact of fluid stratification despite the applications of such a phenomenon. Stratification in fluids happens due to density variation between two fluid layers and can arise as a result of differences in salinity, temperature, or a combination of both. The formation or deposition of layers in a vertical route which is often encountered in various natural, engineering as well as in industrial activities and atmospheres can be described by this term. In practical situations where there is a simultaneous occurrence of heat and mass transfer, the investigation of dual stratification of fluids becomes very useful. Given various applications, Mukhopadhyay et al. [21] engaged Lie group analysis to study stratified boundary layer flow of a Newtonian fluid in a porous moving sheet having a power-law stretching velocity. The authors' report reveals that thermal stratification cools the boundary layer flow region. Daniel et al. [22] scrutinized the impact of thermal stratification on the transport of an electrically conducting nanoliquid past a nonlinear elongated plate with radiation and nonuniform variable thickness. Their study shows that heat transfer at the surface improves while the surface temperature declines with a rise in the thermal stratification term. Reddy and Sreedevi [23] applied Galerkin Finite Element Technique (GFET) to investigate the influence of double stratification in a reactive and thermally radiating flow and heat transfer of nanofluid along a porous stretchable sheet. Decayed temperature and concentration profiles are recorded for the influence of thermal and solutal stratification respectively. The investigation of double stratification in the stagnation-point flow of third-grade fluid over a nonlinear stretchable sheet characterized by uneven thickness was analytically carried out by Hayat et al. [24]. Their analysis showed that heat transfer was diminished by stronger thermal stratification parameter. Such a concept can also be found in Refs [25–27]. However, there has not been any report on the double stratification effects using the tangent hyperbolic fluid with nonlinear thermal radiation and variable thermal conductivity despite such applications. Therefore, the present study aims to investigate the transport characteristics of a quadratic mixed convective tangent hyperbolic fluid over a vertically stretched sheet with thermal and solutal stratification. The thermal field is modelled to contain the influence of nonlinear thermal radiation, viscous dissipation, Joulean heating and temperature-dependent thermal conductivity. The motivation for this study emanates from the engineering and manufacturing applications of the various parameters emerging from the controlling equations as highlighted in the above literature review. The main equations have been effectively tackled using Spectral Local Linearization Method while the contributions of the emerging physical parameters on the dimensionless velocity, temperature, and concentration as well as on the surface drag force and heat transfer analysis have been shown using graphs and tables for application purposes.

2   Problem Formulation

Consider a quadratic mixed convection flow, heat and mass transfer of a tangent hyperbolic fluid characterized by double stratification and nonlinear thermal radiation. The following assumptions are fixed for the development of the problem in the present study.

- The flow is steady, two-dimensional $(x, \ y, \ 0)$, incompressible and laminar flow.

- The temperature within the flow is high such that nonlinear thermal radiation is applicable.

- The thermal conductivity is linearly dependent on the temperature. Viscous dissipation and Joule heating effects are incorporated into the energy equation.

- The flow is directed towards the x-axis in the vertical coordinate with stretching velocity indicated as $u_w = bx$, where $b > 0$ is the stretching rate whereas *the* y-axis is normal to the direction of flow.

- An external magnetic field of uniform strength is applied parallel to the y-axis whereas the impact of the induced magnetic field is ignored owing to the small size of the magnetic Reynolds number.

- The temperature and concentration of the sheet are higher than that of the free stream, i.e. $T_w > T_\infty$ and $C_w > C_\infty$
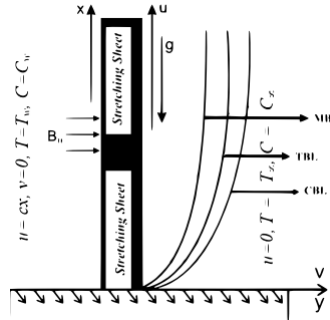

Fig. 1: Flow Configuration

The general form of the nonlinear density variation with temperature and concentration as given by Mandal and Mukhopadhyay [28] as well as Mahanthesh and Mackolil [29] are:

$$\rho\left(T\right) = \rho\left(T_w\right) + \left(\frac{\partial \rho}{\partial T}\right)_w (T - T_w) + \left(\frac{\partial^2 \rho}{\partial T^2}\right)_w (T - T_w)^2 + \ldots,$$

$$\rho\left(C\right) = \rho\left(C_w\right) + \left(\frac{\partial \rho}{\partial C}\right)_w (C - C_w) + \left(\frac{\partial^2 \rho}{\partial C^2}\right)_w (C - C_w)^2 + \ldots,$$

Considering the terms up to the second order in each of the above relations respectively results to

$$\frac{\Delta \rho}{\rho} = -h_1\left(T - T_w\right) - h_2(T - T_w)^2,$$

$$\frac{\Delta \rho}{\rho} = -h_3\left(C - C_w\right) - h_4(C - C_w)^2,$$

where h_1, h_2, h_3 and h_4 are coefficient of linear thermal expansion, coefficient of nonlinear thermal expansion, coefficient of linear solutal expansion and coefficient of nonlinear solutal expansion in that order. The relations above are referred to as nonlinear density temperature and concentration respectively [28–30].

2.1 The Governing Equations

Given the highlighted assumptions above, together with the boundary layer approximations, the governing boundary layer equations for the flow, heat and mass transport of a quadratic mixed convection tangent hyperbolic fluid are specified as follows. (see Refs [31–33]).

$$\frac{\partial u}{\partial x} + \frac{\partial v}{\partial y} = 0 \tag{2.1}$$

$$\vartheta\left(1 - n\right)\frac{\partial^2 u}{\partial y^2} + \vartheta\sqrt{2}n\Upsilon\frac{\partial^2 u}{\partial y^2}\frac{\partial u}{\partial y} - \frac{\sigma B_0^2}{\rho}u + g\left[\begin{array}{c} h_1\left(T - T_\infty\right) + h_2(T - T_\infty)^2 \\ +h_3\left(C - C_\infty\right) + h_4(C - C_\infty)^2 \end{array}\right]$$

$$= \left(u\frac{\partial u}{\partial x} + v\frac{\partial u}{\partial y}\right) \tag{2.2}$$

$$\frac{1}{(\rho c_p)} \frac{\partial}{\partial y}\left(k\frac{\partial T}{\partial y}\right) + \frac{\sigma B_0^2}{\rho c_p} u^2 + \frac{\mu}{\rho c_p}\left((1-n)\left(\frac{\partial u}{\partial y}\right)^2 + \frac{\Upsilon n}{\sqrt{2}}\left(\frac{\partial u}{\partial y}\right)^3\right) + \frac{16\sigma^\star}{3k^\star \rho c_p}\frac{\partial}{\partial y}\left(T^3\frac{\partial T}{\partial y}\right)$$

$$= \left(u\frac{\partial T}{\partial x} + v\frac{\partial T}{\partial y}\right) \tag{2.3}$$

$$u\frac{\partial C}{\partial x} + v\frac{\partial C}{\partial y} = D_b\,\frac{\partial^2 C}{\partial y^2} \tag{2.4}$$

The variation of the thermal conductivity with temperature is taken as [34, 35]:

$$k = \mathrm{k}_\infty\left[1 + \varepsilon\frac{(T-T_\infty)}{(T_w - T_\infty)}\right]. \tag{2.5}$$

Given the governing Eqs. (1-4) together and the dynamics of stratification, the under-listed are the associated boundary conditions:

$$u = u_w = bx, v = 0, T = T_w(x) = T_0 + c_1 x,\ C = C_w(\mathrm{x}) = \mathrm{C}_0 + d_1 x\ when\ y = 0,$$
$$u \to u_0\ , T \to T_\infty(x) = T_0 + c_2 x, C \to C_\infty(x) = C_0 + d_2 x\ as\ y \to \infty \tag{2.6}$$

In the above governing equations, ε indicates the thermal conductivity term which depends on the nature of the fluid, k_∞ denotes the upstream thermal conductivity, *and* $k^\star$ mean absorption coefficient whereas ϑ, D_b C_w, T_w, g, Υ, C_∞, T_∞, u, v sequentially defines the kinematic viscosity, mass diffusivity, wall concentration, wall temperature, gravitational acceleration, velocity in x-direction, velocity in *the* y direction. In the boundary conditions, c_1, c_2, d_1, *and* d_2 describe dimensionless constants. Likewise, B_0, μ, ρ, h_1, h_2, h_3, h_4, c_p, n, $\sigma^\star$ respectively describes magnetic field strength, dynamic fluid viscosity, fluid density, coefficient of linear thermal expansion, coefficient of nonlinear thermal expansion, coefficient of linear concentration expansion, coefficient of nonlinear concentration expansion, specific heat at constant pressure, power law index, Stefan-Boltzmann constant and $T_0(C_0)$ connotes reference temperature (concentration). Due to the influence of thermal stratification the nonlinear radiation term in the energy equation (2.3) is modified as a result of $(T - T_\infty)$ and $(T_w - T_0)$. The temperature T becomes $T = T_\infty\left(1 + \left(\frac{1}{S_\theta + \theta_w}\right)\theta\right)$ where S_θ and θ_w are thermal stratification and temperature ratio terms respectively.

The under-listed dimensionless variables are introduced into the main equations.

$$\eta = \sqrt{\frac{b}{\vartheta}}y, \psi = \sqrt{b\vartheta}xf(\eta), \theta(\eta) = \frac{T-T_\infty}{T_w-T_0}, \mathrm{Rd} = \frac{16\sigma^\star T_\infty^3}{3k^\star k_\infty}, Re = \frac{u_w x}{\vartheta},\ u = bxf'(\eta),$$
$$\phi(\eta) = \frac{C-C_\infty}{C_w-C_0}, u = \frac{\partial\psi}{\partial y}, v = -\frac{\partial\psi}{\partial x},\ S_\theta = \frac{c_2}{c_1}\ ,\ S_\phi = \frac{d_2}{d_1}, \beta_1 = \frac{h_2(T_w-T_0)}{h_1}$$
$$\mathrm{w} = \frac{T_0}{T_w-T_0}\left(or\frac{T_0}{bx}\right), G = \frac{(T_w-T_0)}{T_\infty}, Pr = \frac{c_p}{k_\infty}, M = \frac{\sigma B_0^2}{b\rho}, Gr_x = \frac{g\gamma_1(T_w-T_\infty)x^3}{\vartheta^2}, Sc = \frac{\vartheta}{D_B}, \tag{2.7}$$
$$Gc_x = \frac{gh_3(C_w-C_0)x^3}{\nu^2}, \lambda = \frac{Gr_x}{Re_x^2}, N = \frac{Gc_x}{Gr_x}, We = \Upsilon\sqrt{\frac{2b^3 x^2}{\vartheta}}, \beta_2 = \frac{h_4(C_w-C_0)}{h_3}$$
$$Ec = \frac{u_w^2}{C_p(T_w-T_\infty)}.$$

The substitution of quantities in (2.7) into the governing Eqs. $(1 - 4)$ and the boundary conditions (2.5) lead to automatic satisfaction of Eq. (2.1) and consequently produces the nonlinear ordinary differential equations listed in Eqs. $(8 - 10)$.

2.2 The Transformed Equations

$$\left((1-n) + nWef''\right)f''' + ff'' - f'^2 - Mf' + \lambda\theta(1+\beta_1\theta) + \lambda\,\phi N(1+\beta_2\phi) = 0, \tag{2.8}$$

$$\frac{1}{Pr}\left[1 + \varepsilon\theta + Rd\left(1 + \left(\frac{1}{S_\theta + \theta_w}\right)\theta\right)^3\right]\theta'' + 3Rd\left(1 + \left(\frac{1}{S_\theta + \theta_w}\right)\theta\right)^2\left(\frac{1}{S_\theta + \theta_w}\right)\theta'^2 +$$
$$(f\theta' - f'\theta - S_\theta f') + Ecf''^2\left((1-n) + \frac{nWe}{2}f''\right) + \frac{\varepsilon}{Pr}\theta'^2 + EcMf'^2 = 0, \tag{2.9}$$

$$\frac{1}{Sc}\phi'' + (f\phi' - f'\phi - S_\phi f') = 0. \tag{2.10}$$

Similarly, the associated wall and far stream conditions transform to the underlisted:

$$f'(0) = 1, f(0) = 0, \theta(0) = 1 - S_\theta, \phi(0) = 1 - S_\phi$$

$$f'(\infty) = 0, \theta(\infty) = 0, \phi(\infty) = 0. \tag{2.11}$$

The definitions of the controlling physical parameters featured in Eqs (8-11) are expressed in Eqs (2.7) with We, M, N, λ, β_1, β_2, Pr, Ec, Rd, θ_w, S_θ, S_ϕ and Sc sequentially describes Weissenberg number, magnetic field term, ratio of concentration to buoyancy force parameter, mixed convection parameter, nonlinear thermal convection term, nonlinear concentration convection term, Prandtl number, Eckert number, radiation parameter, temperature ratio term, thermal stratification term, solutal stratification parameter and Schmidt number. For technology and engineering applications, it is imperative to include the physical quantities such as the skin friction coefficient, C_{fx} which describes the viscous drag between the sheet and the fluid, the local Nusselt number, Nu_x corresponding to heat transfer at the surface and then the Sherwood number, Sh_x which describes the mass transfer rate. Eq. (2.12) orderly shows the description of these quantities as

$$C_{fx} = \frac{2\tau_w}{u_w^2}, Nu_x = \frac{xq_w}{k_\infty (T_w - T_0)}, Sh_x = \frac{xq_m}{D_b (C_w - C_0)}, \tag{2.12}$$

where $\tau_w = \left[\frac{\partial u}{\partial y} + \frac{\Upsilon}{\sqrt{2}}\left(\frac{\partial u}{\partial y}\right)^2\right]_{y=0}$, $q_w = -\left[\left(k_\infty + \frac{16T^3\sigma^\star}{3k^\star}\right)\frac{\partial T}{\partial y}\right]_{y=0}$ and $q_w - \left(D_b \frac{\partial C}{\partial y}\right)_{y=0}$

respectively symbolizes the wall shear stress, the surface heat flux and the surface mass flux. The dimensionless quantities related to Eq. (2.12) are listed in Eq. (13-15) as

$$Re_x^{\frac{1}{2}} C_{fx} = \left[(1 + n)f''(0) + \frac{We}{2}f''^2(0)\right], \tag{2.13}$$

$$Re_x^{-\frac{1}{2}} Nu_x = -\left[1 + Rd(1 + (\theta_w - 1)\theta(0))^3\right]\theta'(0), \tag{2.14}$$

$$Re_x^{-\frac{1}{2}} Sh_x = -\phi'(0) \tag{2.15}$$

3 Method of Solution

Difficulty in solving ordinary differential equations or partial differential equations varies depending on the level of non-linearity. The equations could be solved using analytical techniques or numerical methods. However, these methods pose some challenges in their implementation. As per analytical techniques, its challenges could be; slow or non-convergence of obtained solutions to the true solution, solutions being too cumbersome for practical use, non-existence of general analytic methods for non-linear problems, and many difficulties in the solution processes, amongst others. Also, for numerical methods, stability and convergence could be an issue. There could be difficulty in dealing with singularities and it might be uneasy to interpret some numerical results/solutions such as the occurrence of multiple solutions. Hence, there is a need for modifications and improvements of the existing analytical and numerical methods. The quest for optimal methods to address these problems brings about the Spectral Methods. An efficient iterative method known as Spectral Local Linearization Method (SLLM), described by Motsa [36, 37] has been employed to solve the boundary value problem BVP (8-11). Due to the effectiveness of this method, various authors have engaged it to solve various nonlinear BVP. For instance, Ogunseye and Sibanda [38] applied SLLM to study the transport of Powell-Eyring nanofluid in a porous channel with entropy analysis. Ayano et al. [39] applied the SLLM to solve steady mixed convection MHD Casson nanofluid bioconvective flow through a Darcy-Forchheimer porous stratum. Sithole et al. [40] engaged this method

to investigate entropy generation in MHD second-grade nanofluid motion with convective heating and nonlinear thermal radiation effects. The transport of MHD micropolar fluid over a nonlinear elongated porous plate with multiple slips was examined by Fatunmbi et al. [41] via this technique. Recently, Ogunseye et al. [42] reported on the complete exothermic reaction of viscoplastic fluid containing nanoparticles in a cylindrical medium using SLLM. Furthermore, via SLLM, Adigun et al. [43] examined the effect of solutal and thermal stratification, and activation energy on the Stagnation point MHD slip-flow of viscoelastic nanomaterial over a stretched inclined cylindrical surface in a porous medium, with variable fluid properties. In this method, the linearization of all nonlinear terms via one term Taylor series expansion for multiple variables is carried out. Thereafter, the Gauss-Siedel iteration technique is also used to decouple the equations while the Chebyshev Pseudo-spectral technique is applied to tackle those decoupled equations. The non-linear coupled Equations (8 – 10) together with boundary conditions (2.11) would be numerically integrated. Consider the differential operators below:

$$\Phi_f = (1 - n) f_n''' + f_n f_n'' - f_n'^2 + nWe f_n''' \left(f_n'' \right) - M f_n' + \lambda \theta_n \left(1 + \beta_1 \theta_n \right) + \lambda N \phi_n \left(1 + \beta_2 \phi_n \right) \tag{3.1}$$

$$\Phi_\theta = \left(1 + \varepsilon \theta_n + Rd \left(1 + \left(\frac{1}{S_\theta + \theta_w} \right) \theta_n \right)^3 \right) \theta_n'' + 3Rd \left(\frac{1}{S_\theta + \theta_w} \right) \theta_n'^2 \left(1 + \left(\frac{1}{S_\theta + \theta_w} \right) \theta_n \right)^2 + \varepsilon \theta_n'^2$$
$$+ \Pr \left(f_n \theta_n' - f_n' \left(\theta_n + S_\theta \right) \right) + \Pr Ec f_n''^2 \left((1 - n) + \frac{nWe}{2} f_n'' \right) + \Pr Ec M f_n'^2 \tag{3.2}$$

$$\Phi_\phi = \phi_n'' + Sc \left(f_n \phi_n' - f_n' \phi_n - S \phi f_n' \right), \tag{3.3}$$

where prime denotes the derivative with respect to η. Equations (21-23) can be decoupled by implementing the algorithm below:
(a) from Φ_f, find f_{n+1} while treating θ_n and ϕ_n as known functions from the developed initial guess.
(b) solve for θ_{n+1} from Φ_θ, while treating f_n and ϕ_n as known functions, f_n from (a) above and ϕ_n the developed initial guess.
(c) solve for ϕ_{n+1} from Φ_ϕ, while treating f_n and as known functions, f_n from (a) and (b) above respectively.
The non-linear system of equations (16-18) are written as

$$\alpha_{1,n} f_{n+1}''' + \alpha_{2,n} f_{n+1}'' + \alpha_{3,n} f_{n+1}' + \alpha_{4,n} f_{n+1} = R_n^f \tag{3.4}$$

$$\alpha_{5,n} \theta_{n+1}'' + \alpha_{6,n} \theta_{n+1}' + \alpha_{7,n} \theta_{n+1} = R_n^\theta \tag{3.5}$$

$$\alpha_{8,n} \phi_{n+1}'' + \alpha_{9,n} \phi_{n+1}' + \alpha_{10,n} \phi_{n+1} = R_n^\phi \tag{3.6}$$

subject to boundary conditions

$$f_{n+1}(0) = 0, \ f_{n+1}'(0) = 1, \ f_{n+1}'(\infty) = 0$$
$$\theta_{n+1}(0) = 1 - S_\theta(0), \ \theta_{n+1}(\infty) = 0 \tag{3.7}$$
$$\phi_{n+1}(0) = 1 - S_\phi(0), \ \phi_{n+1}(\infty) = 0,$$

where the coefficients $\alpha_{i,n}$ $(i = 1, ..., 8)$, are known functions from previous iterations and are explicitly written out below.

$$\alpha_{1,n} = \frac{\partial \Phi_f}{\partial f_n'''} = nWe f_n'' - n + 1, \alpha_{2,n} = \frac{\partial \Phi_f}{\partial f_n''} = nWe f_n''' + f_n, \alpha_{3,n} = \frac{\partial \Phi_f}{\partial f_n'} = -2f_n' - M, \alpha_{4,n} = \frac{\partial \Phi_f}{\partial f_n} = f_n''$$

$$\alpha_{5,n} = \frac{\partial \Phi_\theta}{\partial \theta_n''} = 1 + \varepsilon \theta_n + Rd \left(1 + (\theta_r - 1) \theta_n \right)^3 \ \alpha_{6,n} = \frac{\partial \Phi_\theta}{\partial \theta_n'} = 6Rd \left(\theta_r - 1 \right) \theta_n'^2 \left(1 + (\theta_r - 1) \theta_n \right)^2 + 2\varepsilon \theta_n' + \Pr f_n$$

$$\alpha_{7,n} = \frac{\partial \Phi_\theta}{\partial \theta_n} = 6Rd \left(\frac{1}{S_\theta + \theta_w} \right) \theta_n'^2 \left(1 + \left(\frac{1}{S_\theta + \theta_w} \right) \theta_n \right)^2 - \Pr f_n'$$

$$\alpha_{8,n} = \frac{\partial \Phi_\phi}{\partial \phi_n''} = 1, \alpha_{9,n} = \frac{\partial \Phi_\phi}{\partial \phi_n'} = Scf_n, \alpha_{10,n} = \frac{\partial \Phi_\phi}{\partial \phi_n} = -Scf_n'$$

$$R_n^f = \alpha_{1,n}f_n'''' + \alpha_{2,n}f_n''' + \alpha_{3,n}f_n'' + \alpha_{4,n}f_n' + \alpha_{5,n}f_n - \Phi_f$$

$$R_n^\theta = \alpha_{6,n}\theta_n'' + \alpha_{7,n}\theta_n' + \alpha_{8,n}\theta_n - \Phi_\theta, R_n^\phi = \alpha_{9,n}\phi_n'' + \alpha_{10,n}\phi_n' + \alpha_{11,n}\phi_n - \Phi_\phi \qquad (3.8)$$

Equations (3.4), (3.5), (3.6) and (3.7) are solved numerically via the Chebyshev pseudo-spectral technique (Canuto et al. [38]). The domain of the problem is transformed to the interval $[-1, 1]$using the transformation$\eta = \frac{1}{2}(\xi + 1)\varpi_\infty$. The unknown functions $f(\eta)$, $\theta(\eta)$ and $\phi(\eta)$ are discretized using the Gauss-Lobatto points

$$\xi_k = \cos\left(\frac{\pi k}{\bar{N}}\right), \quad k = 0, 1, ..., \bar{N}; \quad -1 \leq \xi \leq 1. \qquad (3.9)$$

The differentiation matrix D is used to approximate the derivatives of the unknown variables f_n, θ_n and ϕ_n at the collocation point to the matrix-vector product,

$$\frac{df}{d\eta} = \sum_{i=0}^{\bar{N}} D_{ij}f(\xi_i) = \mathbf{D}F, \quad \frac{d\theta}{d\eta} = \sum_{i=0}^{\bar{N}} D_{ij}\theta(\xi_i) = \mathbf{D}\theta \quad \text{and} \quad \frac{d\phi}{d\eta} = \sum_{i=0}^{\bar{N}} D_{ij}\phi(\xi_i) = \mathbf{D}\phi, \qquad j = 0, 1, 2, ..., \bar{N},$$

$$(3.10)$$

where $\bar{N} + 1$ is the number of collocation points, $\mathbf{D} = 2D/\varpi_\infty$and$F = [f(\xi_0), f(\xi_1), ..., f(\xi_{\bar{N}})]^T$, $\Theta = [\theta(\xi_0), \theta(\xi_1), ..., \theta(\xi_{\bar{N}})]^T$and $\Phi = [\phi(\xi_0), \phi(\xi_1), ..., \phi(\xi_{\bar{N}})]^T$are vector functions at the collocation points. In addition, let Θ and Φ be similar vector functions representing θ and ϕ respectively. Higher order derivatives of f, $\theta$and ϕ are evaluated as powers of $\mathbf{D}$, that is $f^s(\eta) = \mathbf{D}^s F, \theta^s(\eta) = \mathbf{D}^s\Theta$and $\phi^s(\eta) = \mathbf{D}^s\Phi$, for lower case s. The decoupled matrix below is obtained when Equations (3.9), (3.10) and (31) are substituted into (24-27).

$$\begin{bmatrix} \mathbf{D}_{1,1} & ... & \mathbf{D}_{1,\bar{N}+1} \\ \begin{matrix} diag[\alpha_{1,n}]\mathbf{D}^3 + diag[\alpha_{2,n}]\mathbf{D}^2 + diag[\alpha_{3,n}]\mathbf{D} + diag[\alpha_{4,n}]J \\ \mathbf{D}_{\bar{N}-1,1} \\ \mathbf{D}_{\bar{N},1} \\ \mathbf{D}_{1,1} \end{matrix} & \begin{matrix} ... \\ ... \\ ... \end{matrix} & \begin{matrix} \mathbf{D}_{\bar{N}-1,\bar{N}+1} \\ \mathbf{D}_{\bar{N},\bar{N}+1} \\ \mathbf{D}_{1,\bar{N}+1} \end{matrix} \end{bmatrix} \times \begin{bmatrix} f_{n+1}(\xi_0) \\ f_{n+1}(\xi_1) \\ \vdots \\ \vdots \\ f_{n+1}(\xi_{N-1}) \\ f_{n+1}(\xi_N) \end{bmatrix} = \begin{bmatrix} 0 \\ R_{n+1}^f(\xi_1) \\ \vdots \\ \vdots \\ 1 \\ 0 \end{bmatrix}$$

$$\begin{bmatrix} 1 & ... & 0 \\ diag[\alpha_{5,n}]\mathbf{D}^2 + diag[\alpha_{6,n}]\mathbf{D} + diag[\alpha_{7,n}]J \\ 0 & ... & 1 \end{bmatrix} \begin{bmatrix} \theta_{n+1}(\xi_0) \\ \\ \theta_{n+1}(\xi_N) \end{bmatrix} = \begin{bmatrix} 0 \\ R_{n+1}^\theta(\xi) \\ \vdots \\ S_\theta \end{bmatrix}$$

$$\begin{bmatrix} 1 & ... & 0 \\ diag[\alpha_{8,n}]\mathbf{D}^2 + diag[\alpha_{9,n}]\mathbf{D} + diag[\alpha_{10,n}]J \\ 0 & ... & 1 \end{bmatrix} \begin{bmatrix} \phi_{n+1}(\xi_0) \\ \\ \phi_{n+1}(\xi_N) \end{bmatrix} = \begin{bmatrix} 0 \\ R_{n+1}^\phi(\xi) \\ \vdots \\ S_\phi \end{bmatrix}.$$

where, $J$is an $(\bar{N}+1) \times (\bar{N}+1)$identity matrix, and $diag[]$denotes a diagonal matrix. The initial approximations taken for the SLLM implementation are

$$f_0(\eta) = 1 - e^{-\eta}, \; \theta_0(\eta) = \left(\frac{1}{1-S_\theta}\right)e^{-\eta} \; \text{and} \; \phi_0(\eta) = \left(\frac{1}{1-S_\phi}\right)e^{-\eta}$$

Table 1 shows the convergence analysis for the developed numerical scheme that was used to solve the governing equations. The convergence of solutions is noticed from the 7th iteration, as subsequent iterations no longer have any effects on the results obtained for momentum, energy, and

concentration equations. The accuracy of the current result has been checked by validating the computational values of the skin friction coefficient for various values of the magnetic field term M with the existing study of Fathizadeh et al. [40] under some limiting conditions A good agreement exists in the comparison as recorded in Table 2.

Table 1: Numerical scheme convergence for variation in the number of iterations

Number of iterations	C_{fx}	Nu_x	Sh_x
1	-1.25065217	1.13786499	1.46167328
5	-1.25503222	1.13260153	1.45894040
7	-1.25503235	1.13260135	1.45894030
8	-1.25503235	1.13260135	1.45894030
9	-1.25503235	1.13260135	1.45894030

Table 2: Computed values of the skin friction coefficient C_{fx} compared with existing studies for variation in M when other parameters are zero

M	Fathizadeh et al. [44]	Present (SLLM)	Absolute Difference
1	-1.41421	-1.41421356	3.56×10^{-6}
5	-2.44948	-2.44948974	9.74×10^{-6}
10	-3.31662	-3.31662479	4.79×10^{-6}
50	-7.14142	-7.14142843	8.34×10^{-6}
500	-10.0499	-10.04987543	2.46×10^{-5}

3.1 Convergence and Stability Analysis

In order to validate the accuracy of the numerical results obtained from the SLLM, the error norms may be used to evaluate the convergence and stability of the iterative scheme. To achieve this,

- the effect of collocation (grid) points on the accuracy of the solutions obtained is observed to understand if an increase in the number of collocation points affected the accuracy of solutions obtained.

- the effect of the number of iterations on the accuracy of the solutions obtained is observed, to understand if an increase in the number of collocation points affected the accuracy of solutions obtained.

The infinity norms are used to identify the extent by which approximate solutions of $Res\left(f\right)$, $Res(\theta)$ and $Res(\phi)$ deviate from the real solution. These are defined as $IN_r\left(f\right) = \|Res(f)\|_{\infty}$, $IN_r\left(\theta\right) = \|Res(\theta)\|_{\infty}$ and $IN_r\left(\phi\right) = \|Res(\phi)\|_{\infty}$. The point when the values of the error norms obtained from the iterations don't change any longer is referred to as a "point of optimal residual". When applying the method, it was observed that their algorithm was easy to set up and gave very accurate results with few grid points. The convergence rate of the method was observed to be high and its accuracy was very impressive. However, the like work done by Sithole *et al.* [40], who presented an analysis of the residual errors to show the accuracy and convergence of the SLLM, the graphs below describe the residual errors involved in the numerical computation.
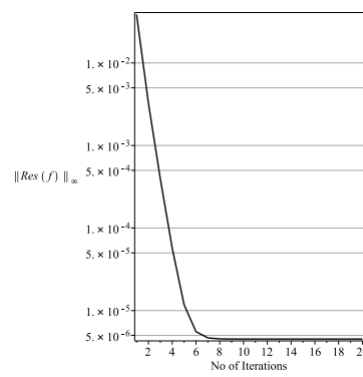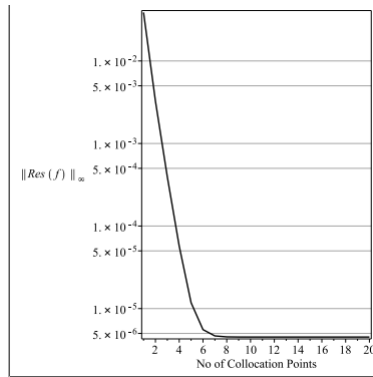
Fig.2 Collocation points on $\|Res(f)\|_\infty$ **Fig. 3** Number of iterations on $\|Res(f)\|_\infty$

Fig. 2 unveils the behaviour of the residual error against the number of collocation points and they all show that as collocation points increase, the residual error decreases. The maximum residual error is attained at about 8 collocation points. The trend is similar in Fig. 3. It shows that the number of iterations at some point, no longer has any effect on the residual error when it is already optimized. That optimal residual is noticed at about 8 iterations.

4   Results and Discussion

This section graphically highlights the significant contributions of some of the physical parameters on the non-dimensional quantities: velocity profile, temperature field and concentration profile. Besides, the effects of some key parameters on the skin friction coefficient, Nusselt number and Sherwood number are also analyzed and publicized accordingly through various tables.
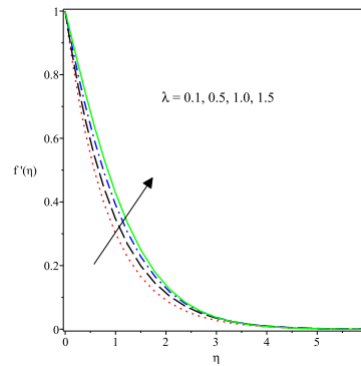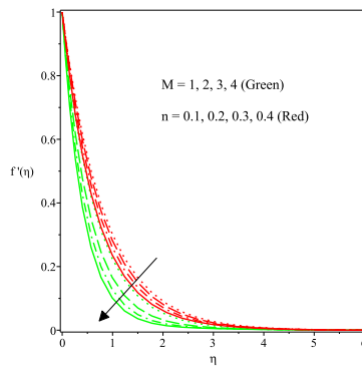

Fig.4 Variation of $M\&n$ on the velocity profile   **Fig.5** Plot ofλ on the velocity field

The effects of both magnetic field term M and power law index n on the velocity profile are described in Fig. 4. The fluid motion decelerates for both parameters as found in this plot. The interaction of the electro-conducting tangent hyperbolic fluid and the transverse magnetic field induces a retarding force known as the Lorentz force. This force resists the fluid movement as M is being increased in magnitude and thereby, a decelerating flow occurs. Similarly, a retarding flow occurs due to an increase in n. Growing values of n depict a rise in the fluid viscosity and as such, there is a resistance to the fluid motion. Thus, the nature of the fluid changes from shear thinning to shear thickening and in consequence, the hydrodynamic boundary layer shrinks and the velocity is reduced. On the other hand, the fluid motion accelerates with a rise in the mixed convective variable parameter, λ as demonstrated in Fig. 5. The mixed convective parameter describes the ratio of the buoyancy force to viscous force, thus an enhancement in aids the buoyancy force and strengthens it over the viscous force. Such a phenomenon leads to the thickening of the hydrodynamic boundary layer and better fluid acceleration since the viscous force is reduced.
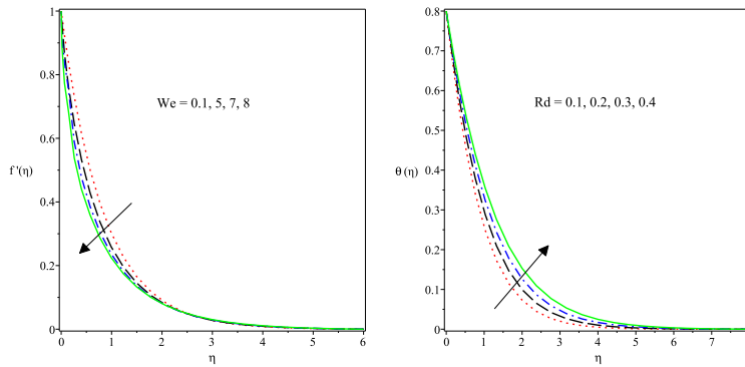
Fig.6 Variation of We on the velocity profile   **Fig.7** Plot of Rd on temperature profiles

Fig. 6. is a description of the reaction of the velocity profile to variation in the tangent hyperbolic material parameter (Weissenberg number) We. A rise in We shrinks the momentum boundary structure and decelerates the fluid motion as displayed in this figure. The material term We is directly proportional to the relaxation time of the fluid and as such, a rise in We favours the relaxation time which consequently offers greater resistance to the fluid motion. There is an increase in the surface temperature as the thermal radiation term Rd increases as found in Fig. 7. With an increase in Rd, the mean absorption coefficient reduces and thus thickens the thermal boundary layer and the temperature is also raised. Likewise, the surface temperature escalates with growth in the value of the temperature parameter θ_w as sketched in Fig. 8. This parameter describes the ratio of the sheet temperature to that of the upstream temperature $\left(\theta_w = \frac{T_w}{T_\infty}\right)$ and it is also known as the wall heating parameter. As θ_w increases, the operating temperature at the wall is encouraged in the flow region as, hence, the thermal state of the fluid is enhanced, leading to a rise in the temperature. The description of the impact of Eckert number Ec on the heat distribution is seen in Fig. 9. An Eckert number is a dimensionless quantity which describes the ratio of the kinetic energy to the enthalpy. It reveals the impact of internal heating of a fluid due to internal friction. Thus, a rise in Ec leads to additional heating which is responsible for a rise in the temperature. For the effect of the thermal stratification parameter S_θ, Fig. 10 elucidates the declining nature of the thermal field due to a rise in S_θ. A rise in this term produces a denser density of the fluid in the lower region in comparison to the upper region. Consequently, the temperature difference between the heated surface and the upstream region becomes reduced which leads to a decline in the fluid temperature. Fig. 11 depicts the graph of the concentration, $\phi(\eta)$ versus η for variation in the Schmidt number, Sc. It is found that a rise in Sc causes the concentration profile to diminish. This parameter (Sc) describes the ratio of the momentum diffusivity and mass diffusivity. Thus, with growing values of Sc, the mass diffusivity is reduced and consequently the solutal boundary layer and the concentration profile decline.
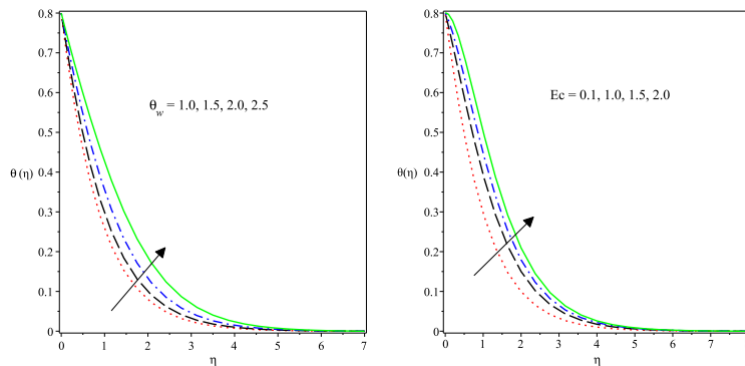

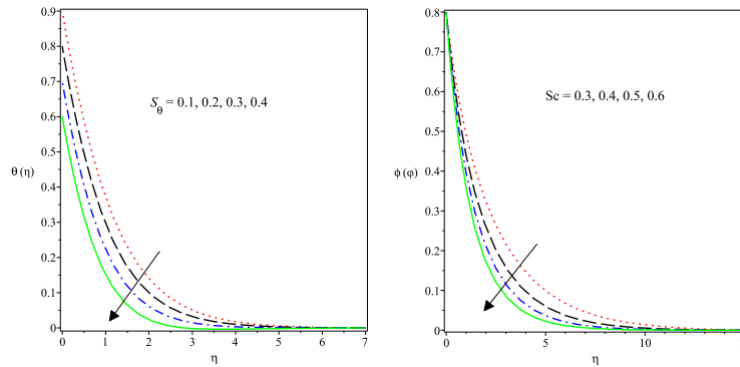**Fig.8** Temperature profiles for changes in θ_w **Fig.9** Temperature profiles for varying Ec

Fig.10 Temperature profiles for changes in S_θ **Fig.11** Concentration profiles for Sc

Table 3: Numerical values of the skin friction coefficient for different values of n, M, We, λ, N, β_1 and β_2

n	M	We	λ	β_1	N	β_2	$-Re_x^{\frac{1}{2}}C_{fx}$
0.1	0.4	0.1	0.1	0.1	0.1	0.1	1.11505710
0.2							1.18648639
0.3							1.27520668
	1						1.45513233
	2						1.79701900
	3						2.08628443
		0.1					1.11505710
		0.5					1.13325856
		1.0					1.15839606
			0.1				1.11505710
			0.5				0.94748743
			1.0				0.75282335
				0.1			1.11505710
				0.2			1.11297699
				0.3			1.11089839
					0.1		1.11505710
					0.5		1.10371834
					0.9		1.09241696
						0.1	1.11505710
						0.2	1.11491752
						0.3	1.11477794

In Table 3, the impact of some chosen parameters n, M, We, λ, β_1, N and β_2 on the skin friction coefficient which corresponds to surface friction as a result of the drag between the fluid and the stretching surface are checked. As noted in this table, the values of the skin friction coefficient are all negative for all the parameters checked. Such a phenomenon occurs when the stretching plate drags the fluid against the fluid dragging the plate. It is observed that a rise in the power law index n raises the frictional drag due to the fact the fluid becomes more viscous with higher values of n. A hike in the values of M also boosts the skin friction coefficient due to resistance in the flow resulting from the Lorentz force. Growth in the Weissenberg number, We also induces a rise in the skin friction coefficient due to an increase in the viscosity of the fluid. On the other hand, the skin friction coefficient reduces as λ, β_1, N and β_2 improve in magnitude.

Table 4: Numerical values of $Re_x^{-\frac{1}{2}}Nu_x$ and $Re_x^{-\frac{1}{2}}Sh_x$ for different values of ε, M, We, Pr, Ec, Sc, S_θ and S_ϕ when $\lambda = \beta_1 = \beta_2 = N = 0.1$

ε	M	We	Pr	Ec	Sc	S_θ	S_ϕ	$Re_x^{-\frac{1}{2}} Nu_x$	$Re_x^{-\frac{1}{2}} Sh_x$
0.1	0.2	0.1	1.5	0.1	2	0.2	0.2	0.78640455	1.3929987
0.2								0.75963706	1.39334377
0.3								0.73500512	1.39368708
	1							0.70005442	1.30275142
	2							0.61988997	1.21629325
	3							0.55815502	1.14717629
		0.1						0.78640455	1.39299873
		0.5						0.78481686	1.38986986
		1.0						0.78269178	1.38571648
			0.1					0.60512337	1.39840104
			0.2					0.68126682	1.39584538
			0.3					0.78640455	1.39299873
				1.0				0.47892776	1.39622913
				1.5				0.30572966	1.39805037
				2.0				0.13075632	1.39989123
					0.3			0.78825422	0.40350658
					0.4			0.78794462	0.48496297
					0.5			0.78768500	0.56224846
						0.2		0.78640455	1.39299873
						0.3		0.77283347	1.38993192
						0.4		0.75756055	1.38692767
							0.2	0.78640455	1.39299873
							0.3	0.78624662	1.34291223
							0.4	0.78609006	1.29280704

In Table 4, the response of the Nusselt number (ratio of convective to conductive heat transfer on the surface) and Sherwood (ratio of convective to diffusive mass transfer at the surface) number to variations in some selected parameters ε, M, We, Pr, Ec, Sc, S_θ and S_ϕ are investigated. It is evident from this table that the Nusselt number is a decreasing function of the thermal conductivity parameter ε, magnetic field term M, Weissenberg number We. A rise in the magnitude of these terms implies a lowering of the heat transfer across the sheet surface. However, the case is different when the Prandtl number is increased. The Prandtl number, Pr denotes a dimensionless quantity which approximates the ratio of momentum diffusivity to thermal conductivity. In problems that relate to heat transfer, Pr controls the relative thickness of the momentum diffusivity and thermal boundary layers. As found in this table a rise in Pr propels an improvement in the heat transfer due to a rise in the Nusselt number. More so, the Nusselt number depreciates with growing values of the Eckert number, Ec and thermal stratification parameter, S_θ as noted in Table 4. Ec signals the kinetic energy to the enthalpy of a fluid and it characterizes the impact of internal heating of a fluid due to dissipation (internal friction) effects. Thus, a rise in Ec corresponds to an additional heating effect and a rise in the temperature as such. Heat transfer therefore declines. The thermal stratification phenomenon occurs when two kinds of steam with different temperatures come into contact. Thus, as clearly revealed in Table 4, the thermal stratification term S_θ lowers the transfer of heat. This reaction agrees well with the results of Hayat et al. [45] and Atif et al. [46].

5   Conclusion

This research investigated the mixed convective transport mechanism of a tangent hyperbolic fluid over a vertical stretchy sheet with stratification effects, nonlinear thermal radiation, viscous dissipation and quadratic Boussinesq approximation. The main equations governing the dynamics of flow, heat and mass transfer are restructured into ordinary differential equations via suitable similarity variables and then integrated using SLLM. Comparison with some existing studies reveals an excellent agreement with the current work. The findings are parametrically displayed in various

graphs with appropriate analysis and discussions. More so, the impact of some crucial parameters on the physical quantities of engineering interest are tabulated and discussed effectively for meaningful practical engineering and technological applications. In summary, the under-listed facts are deduced from the investigation:

- Heat transfer can be improved by increasing the values of the Prandtl number whereas the converse is true in the presence of thermal stratification, variable thermal conductivity, viscous dissipation, and tangent hyperbolic fluid material parameter.

- The surface drag force enhanced due to a rise in the power law index, magnetic field influence, and the Weissenberg number while it declined due to the mixed convective term, nonlinear thermal and concentration terms are increased.

- There is a reduction in the hydrodynamic boundary layer and the fluid motion is decreased due to the influence of the Weissenberg number, magnetic field term and power law index whereas an increase in the velocity as the mixed convective variable term upsurges.

- The thermal boundary layer structure and the surface temperature appreciate with growth in the magnitude of nonlinear thermal radiation term, viscous dissipation and thermal radiation parameter.

Nomenclature

B_0	magnetic field strength $[Wbm^{-2}]$	ϵ	thermal conductivity parameter
h_1	linear thermal expansion coefficient $[K^{-1}]$	λ	mixed convection parameter
c_p	specific heat capacity $[J/kgK]$	N	ratio of concentration to buoyancy force
Ec	Eckert number	β_1	nonlinear thermal convection term
f	non-dimensional stream function	η	similarity variable
h_2	nonlinear thermal expansion coefficient $[K^{-1}]$	θ	dimensionless temperature
h_3	linear solutal expansion coefficient $K^{-1}]$	β_2	nonlinear solutal term
g	acceleration due to gravity	S_ϕ	Solutal stratification term
h_4	nonlinear solutal expansion coefficient $[K^{-1}]$	μ	dynamic viscosity $[kgm^{-1}s^{-1}]$
k	thermal conductivity $[Wm^{-1}K^{-1}]$	ϑ	kinematic viscosity $[m^2s^{-1}]$
We	Weissenberg number	ρ	fluid density $[kgm^{-3}]$
$k^\star$	mean absorption coefficient $[m^{-1}]$	D_b	Mass diffusivity $[m^2s^{-1}]$
M	magnetic field parameter	σ_0	electrical conductivity $[Sm^{-1}]$
Rd	radiation parameter	ϕ	dimensionless concentration
Nu_x	Nusselt number	ψ	stream function $[m^2s^{-1}]$
Pr	Prandtl number	S_θ	thermal stratification term
n	Power law index	Sc	Schmidt number
θ_w	temperature ratio parameter	T_0	reference temperature $[K]$
q_w	surface heat flux $[Wm^{-2}]$	C_0	reference concentration $[mol\ m^{-3}]$
C	concentration $[mol\ m^{-3}]$	q_m	surface mass flux $[Wm^{-2}]$
T	temperature $[K]$		
T_w	surface temperature $[K]$		**subscripts**
T_∞	free stream temperature $[K]$	w	surface conditions
u	velocity in x direction $[ms^{-1}]$	∞	free stream conditions
v	velocity in y direction $[ms^{-1}]$		
γ	relaxation time $[s^{-1}]$		

References

[1] Al-Khaled, K. Ullah, S. and Khan, I. Chemically reactive bioconvection flow of tangent hyperbolic nanoliquid with gyrotactic microorganisms and nonlinear thermal radiation, Heliyon 6 (2020) e03117.

[2] Fatunmbi, E. O. and Okoya, S. S. Heat Transfer in Boundary Layer Magneto-Micropolar Fluids with Temperature-Dependent Material Properties over a Stretching Sheet, Advances in Materials Science and Engineering, 2020, Article ID 5734979, 11 pages https://doi.org/10.11552020/573497 9

[3] J. A. Adigun, A. Adeniyan, M. G. Sobamowo. Stagnation point MHD flow of viscoelastic nanofluid past a circular cylinder with non-Fourier heat flux and variable properties. *International Journal of Mechanical & Mechatronics Engineering,* 19(6): 145-160, (2019).

[4] Jabeen, S., Hayat, T., Qayyum, Q. Alsaedi, A. Significance of activation energy in stratified flow of tangent hyperbolic fluid, International Journal of Numerical Methods for Heat & Fluid Flow, 29(8), 2019

[5] Ullah, Z, Gul Zaman, G. and Ishak, A. Magnetohydrodynamic tangent hyperbolic fluid flow past a stretching sheet, Chinese Journal of Physics ,66 (2020) 258-268.

[6] Mahdy, A. Entropy generation of tangent hyperbolic nanofluid flow past a stretched permeable cylinder: Variable wall temperature, Proc IMechE Part E: J Process Mechanical Engineering 0(0), DOI: 10.1177/0954408918774898.

[7] Salahuddin, T, Malik, M. Y., Hussain, A. and Bilal, S. and Awais, M. Effects of transverse magnetic field with variable thermal conductivity on tangent hyperbolic fluid with exponentially varying viscosity, AIP Advances, 5 (2015), doi: 10.1063/1.4937366.

[8] Ibrahim, W. Magnetohydrodynamics (MHD) flow of a tangent hyperbolic fluid with nanoparticles past a stretching sheet with second order slip and convective boundary condition, Results in Physics 7 (2017) 3723-3731.

[9] Adeniyan, A and Adigun, J. A. Similarity solution of hydromagnetic flow and heat transfer past an exponentially stretching permeable vertical sheet with viscous dissipation, Joulean and viscous heating effects. Annals of Faculty Engineering Hunedoara:International Journal of Engineering, (2016) 1584-2665.

[10] Adeniyan, A and Adigun, J. A. Stress-work and chemical reaction effects on MHD forced convection heat and mass transfer slip-flow towards a convectively heated plate in a non-Darcian porous medium with surface mass-flux. International Journal of Mathematical Analysis and Optimization: Theory and Applications, (2018) 338-355.

[11] Alao, F. I., Boneze, C. U., Fagbade. F. I. Soret and Dufour effects on heat and mass transfer of boundary layer flow over porous wedge with thermal radiation: bivariate spectral relaxation method. American Journal of Chemical Engineering. 7(1), (2019), 7-21. doi: 10.11648/j.ajche.20190701.12

[12] Kumar, K. G., Ramesh, G. K., Gireesha, B. J. and Rashad, A. M. On stretched magnetic flow of Carreau nanofluid with slip effects and nonlinear thermal radiation, Nonlinear Engineering 2019; 8: 340–349.

[13] Rana, P., Shukla, N., Beg, O. A., Kadir, A and Singh, B Unsteady electromagnetic radiative nanofluid stagnation-point flow from a stretching sheet with chemically reactive nanoparticles, Stefan blowing effect and entropy generation, J Nanomaterials, Nanoengineering and Nanosystems, (2018), 1–14, DOI: 10.1177/2397791418782030

[14] Fatunmbi, E. O. and Adeniyan, A. Nonlinear thermal radiation and entropy generation on steady flow of magneto-micropolar fluid passing a stretchable sheet with variable properties, Results in Engineering 6 (2020) 100142.

[15] Gbadeyan, J. A., Titiloye, E. O., Adeosun, A. T. Effect of variable thermal conductivity and viscosity on Casson nanofluid flow with convective heating and velocity slip, Heliyon 6 (2020) e03076.

[16] T.A. Yusuf, F. Mabood b, W.A. Khan, J.A. Gbadeyan. Irreversibility analysis of Cu-TiO2-H2O hybrid-nanofluid impinging on a 3-D stretching sheet in a porous medium with nonlinear radiation: Darcy-Forchheimer's model, Alexandria Eng. J. (2020), https://doi.org/10.1016/j.aej.20.09.053.

[17] Fatunmbi, E. O., Adeosun, A. T. and Salawu, S. O. Irreversibility Analysis for Eyring–Powell Nanoliquid Flow Past Magnetized Riga Device with Nonlinear Thermal Radiation, Fluids 2021, 6, 416. https://doi.org/10.3390/fluids6110416.

[18] Fatunmbi, E. O., Mabood, F., Elmonser, H. Tlili, I. Magnetohydrodynamic nonlinear mixed convection flow of reactive tangent hyperbolic nano fluid passing a nonlinear stretchable surface, Phys. Scr. 96 (2021) 015204. https://doi.org/10.1088/1402-4896/abc3e9

[19] Patil, P. M., Kulkarni, M., Hiremath, P. S. Nonlinear Mixed Convection Flow of Nanofluid Past a Moving Vertical Slender Cylinder Arabian Journal for Science and Engineering, https://doi.org/10.1007/s13369-019-04286-8

[20] Alsaedi, A., Hayat, T., Qayyum, S., Yaqoob, R. Eyring–Powell nanofluid flow with nonlinear mixed convection: Entropy generation minimization, Computer Methods and Programs in Biomedicine 186 (2020) 105183

[21] Mukhopadhyay, S., Mondal, I. C., and Gorla, R. S. R. Effects of thermal stratification on flow and heat transfer past a porous vertical stretching surface, Heat Mass Transfer (2012) 48:915–921, DOI 10.1007/s00231-011-0930-5

[22] Daniel, Y. S., Aziz, Z. A., Ismail, T. Z. and Salah, F. Thermal stratification effects on MHD radiative flow of nanofluid over nonlinear stretching sheet with variable thickness, Journal of Computational Design and Engineering 5 (2018) 232–242.

[23] Reddy, P. S. and Sreedevi, P. Impact of chemical reaction and double stratification on heat and mass transfer characteristics of nanofluid flow over porous stretching sheet with thermal radiation, International Journal of Ambient Energy, DOI: 10.1080/01430750.2020.1712240.

[24] Hayat, T. and Alsaedi, A. Darcy-Forchheimer flow with nonlinear mixed convection, Appl. Math. Mech. Engl. Ed., 41, 1-12 (2020), doi.org/10.1007/s10483-020-2680-8.

[25] Sarojamma, G., Lakshmi, R. V., Sreelakshmi, K. Vajravelu, K. Dual stratification effects on double-diffusive convective heat and mass transfer of a sheet-driven micropolar fluid flow, Journal of King Saud University – Science 32 (2020) 366–376.

[26] Rehman, K. U., Malik, M. Y., Salahuddin, T and Naseer, M. Dual stratified mixed convection flow of Eyring-Powell fluid over an inclined stretching cylinder with heat generation/absorption effect, AIP Advances 6, 075112 (2016).

[27] Hayat, T., Qayyum, S., Alsaedi, A., Ahmad. B. Mechanisms of double stratification and magnetic field in flow of third grade fluid over a slendering stretching surface with variable thermal conductivity, Results in Physics 8 (2018) 819–828.

[28] Mandal, I. C., and Mukhopadhyay, S. Nonlinear convection in micropolar fluid flow past an exponentially stretching sheet in an exponentially moving stream with thermal radiation, Mechanics of Advanced Materials and Structures, (2018). DOI:10.1080/15376494.2018.1472325.

[29] Mahanthesh, B. and Mackolil, J. Flow of nanoliquid past a vertical plate with novel quadratic thermal radiation and quadratic Boussinesq approximation: Sensitivity analysis, Int Comm Heat and Mass Transfer, https://doi.org/10.1016/j.icheatmasstransfer.2020.105040

[30] Fatunmbi, E. O. and Okoya, S. S. Quadratic Mixed Convection Stagnation-Point Flow in Hydromagnetic Casson Nanofluid over a Nonlinear Stretching Sheet with Variable Thermal Conductivity, Defect and Diffusion Forum, 409, 95-109 (2020).

[31] Mamatha, S. U. Raju, C.S. K., Mahesha, and Makinde. O. D. Radiative and viscous Ohmic dissipation on MHD tangent hyperbolic fluid over a convectively heated Sheet in a suspension of dust particles, Diffusion Foundations, 16, 177-190, (2018).

[32] Nayak, M. K., Shaw, S., Makinde, O. D. and Chamkha, A.J. Investigation of partial slip and viscous dissipation effects on the radiative tangent hyperbolic nanofluid flow past a vertical permeable Riga plate with internal heating: Bungiorno model, *Journal of Nanofluids,* 1–12, (2019).

[33] Khan, M. I. Khan, T. A., Qayyum, S. Hayat, T. Khan, M. I and Alsaedi, A. Entropy generation optimization and activation energy in nonlinear mixed convection flow of a tangent hyperbolic nanofluid, Eur. Phys. J. Plus (2018) 133: 329.

[34] Chiam, T. C. Heat transfer with variable thermal conductivity in a stagnation point flow towards a stretching sheet. Int. Commun. Heat Mass Transf. 23, 239–248 (1996).

[35] Akinbobola, T. E. and Okoya, S. S. The flow of second grade fluid over a stretching sheet with variable thermal conductivity and viscosity in the presence of heat source/sink, Journal of the Nigerian Mathematical Society 34 (2015) 331–342.

[36] Motsa, S. S. A new spectral local linearization method for non-linear boundary layer flow problems. Hindawi Publishing Group: Journal of Applied Mathematics. 2013, 15 pages, http://dx.doi.org/10.1155/2013/423628

[37] Motsa, S. S., Dlamini, P. G. and Khumalo. M. Spectral relaxation method and spectral quasi-linearization method for solving unsteady boundary layer flow problems. Advances in Mathematical Physics, (2014) Article ID 341964, 12 pages.

[38] H. A. Ogunseye, P. Sibanda A mathematical model for entropy generation in a Powell-Eyring nanofluid flow in a porous channel, Heliyon 5 (2019) e01662

[39] Ayano, M. S., Magagula, V. M., Mathunjwa, J. S. (2020). Spectral local linearization method for MHD Casson fluid on stratified bioconvective porous medium flow due to gyrotactic microorganisms. Heat Transfer. 2020;1–21. https://doi.org/10.1002/htj.21934

[40] Sithole, H., Mondal, H. and Sibanda, P. Entropy generation in a second grade magnetohydrodynamic nanofluid flow over a convectively heated stretching sheet with nonlinear thermal radiation and viscous flow. Results in Physics 9 (2018) 1077–1085.

[41] E. O. Fatunmbi, H. A. Ogunseye, P. Sibanda. Magnetohydrodynamic micropolar fluid flow in a porous medium with multiple slip conditions, International Communications in Heat and Mass Transfer 115 (2020) 104577.

[42] H.A. Ogunseye, S. O. Salawu, E. O. Fatunmbi A numerical study of MHD heat and mass transfer of a reactive Casson–Williamson nanofluid past a vertical moving cylinder, Partial Differential Equations in Applied Mathematics 4 (2021) 100148.

[43] Adigun, J. A., Adeniyan, A. and Abiala, I. O (2021): Stagnation point MHD slip-flow of viscoelastic nanomaterial over a stretched inclined cylindrical surface in a porous medium with dual stratification. International Communications of Heat and Mass Transfer, 126(2021) 105479

[44] Fathizadeh, M., Madani, M., Khan, Y., Faraz, N., Yıldırım, A. and Tutkun, S. J. King. Saud. University Sci. doi: 10.1016/j.jksus.2011. 08.003 (2013).

[45] Hayat, T., Qayyum, S., Alsaedi, A., B. Ahmad. Mechanisms of double stratification and magnetic field in flow of third grade fluid over a slendering stretching surface with variable thermal conductivity, Results in Physics 8 (2018) 819–828.

[46] Atif, S. M., Hussain, S. and M. Sagheer, M. Magnetohydrodynamic stratified bioconvective flow of micropolar nanofluid due to gyrotactic microorganisms, AIP Advances 9, 025208 (2019); doi: 10.1063/1.5085742